This article has been accepted for publication in a future issue of this journal, but has not been fully edited. Content may change prior to final publication. Citation information: DOI10.1109/TAP.2022.3164885, IEEE Transactions on Antennas and Propagation

Light-Weight Low-Cost Tightly Coupled Dipole Array Antenna for Wireless Power Transfer

Lehu Wen, Benito Sanz-Izquierdo, Wei Hu, *Senior Member, IEEE*, Cong Lin, and Chao Wang

***Abstract*—A light-weight low-cost tightly coupled dipole array (TCDA) antenna is presented for wireless power transfer. A simple low-cost H-plane scanning booster (HSB) layer is first introduced to improve the scanning ability in H-plane. Therefore, a consistent E- and H-plane scanning performance is achieved for the designed unit cell. In addition, a new 1to4 differential feed network using power dividers and exponentially tapered baluns is designed and utilized to excite the unit cell. Finally, a 5×13 finite array antenna prototype was designed, fabricated, and measured for wide beam scanning performance verification. Both the measured and simulated results confirm that the fabricated array antenna can have a wide and consistent scanning range of ±50° in both E-plane and H-plane over 4.3:1 impedance bandwidth. In addition, low cross-polarization levels of less than -30.5 dB are achieved for the fabricated low top-to-ground profile ($0.4\lambda_h$) TCDA antenna.**

***Index Terms*—Array antenna, differential feed, light weight, low profile, tight coupling, ultrawideband.**

I. Introduction

Wireless power transfer (WPT) is a transformative technology that can significantly change our lives. It can not only be used in the ordinary consumer electronics and new-energy vehicles, but also used in the national defense and space systems [1]. To realize a swift tracking for the remote mobile receivers with high efficiency, far-field remote WPT is utilized and the antennas are required with beam scanning performance for dynamic tracking [2]-[3]. In addition to the wireless power transmission, the related communications between the transmitter and receivers are also needed to be established to ensure the stable link [4]. Therefore, to achieve high WPT efficiency and bandwidth, broadband antennas such as the ultrawideband tightly coupled dipole array (TCDA) antennas are especially a good option for WPT applications.

Normally, by forming Wheeler's current sheet antenna array [5]-[6], classic TCDA antennas can be realized with wide impedance bandwidth and scanning ranges. Various TCDA antennas have been developed with excellent performances [7]-[13]. In these designs, a wide beam scanning range of up to ±60° in E-plane can be achieved. However, in terms of H-plane scanning range, it is either narrower than E-plane or has a deteriorated VSWR, which is undesirable for TCDA antennas. To keep a consistent scanning performance in both E-plane and H-plane, an easy way is adding a thick dielectric superstrate [14]-[17], which works as a wide-angle impedance matching layer to improve the beam scanning performance. However, this will incur a high profile and heavy weight of the antenna. Additionally, FSS-based superstrates [18]-[19], metamaterials [20]-[22], and polarization selective absorbers [23] are utilized for beam scanning improvement. However, these FSS-based superstrates or metamaterials require a certain distance or length to take effect, and it is also normally around a quarter of the wavelength at the highest working frequency.

In this letter, a light-weight, low-cost, and low top-to-ground profile TCDA antenna is proposed for WPT applications. It can not only realize a consistent wide beam scanning performance in E-plane and H-plane, but also has the advantage of avoiding the traditional high-mass dielectric or high-profile FSS-based superstrates for scanning performance improvement. First in this work, an H-plane scanning booster (HSB) layer is proposed to improve the impedance bandwidth when scanning to the large angles. In addition, a new 1to4 differential feed network is designed to excite the unit cell, and its 5×13 finite array antenna was then developed, fabricated, and measured with UWB (4.3:1), consistent scanning ranges of ±50° in both E-plane and H-plane, and low cross-polarization levels (<-30.5 dB).

II. Unit Cell Design

A. Unit Cell Configuration

Fig. 1 shows the detailed configuration of the proposed TCDA unit cell. As shown in Fig. 1 (a), the unit cell is composed of the top radiator, center ground plane, and bottom feed network (power dividers and balun). The periodical length of the square unit cell is 20 mm, which is $0.53\lambda_h$, where λ_h is the freespace wavelength at the highest working frequency of 8 GHz. Fig. 1 (b) shows the top view (xy-plane) of the unit cell. As can be seen, above from the center tightly coupled dipole arms, an HSB layer with the strip length of 13 mm and width of 0.5 mm is symmetrically arranged beside the center dipole, which is used to improve the H-plane scanning capability.

Fig. 1 (c) shows the side view of the proposed unit cell. It is a dual-set configuration for the ease of impedance transforming [15]. There are two dipoles in the unit cell, and the center arm is shared by two dipoles. This shared-arm concept is originated from our previous design in [24], which brings a new form of TCDA structure and aims to reduce the coupling complexity in

This work was supported by Brunel Research Initiative and Enterprise Fund, Engineering and Physical Sciences Research Council under Grant EP/S005625/1, and 111 Project of China. (Corresponding author: Lehu Wen)

L. Wen is with the Department of Electronic and Electrical Engineering, Brunel University London, Uxbridge, UB8 3PH, U.K. (LehuWen@ieee.org)

B. Sanz-Izquierdo and Chao Wang is with the School of Engineering and Digital Arts, University of Kent, Canterbury, CT2 7NT, U.K.

W. Hu and Cong Lin are with the National Key Laboratory of Antennas and Microwave Technology, Xidian University, Xian, 710071, China.

the unit cell. Each dipole is differentially fed by two 50Ω microstrip lines to realize unidirectional radiation. The distance between the top dipole arm and ground plane is 15mm, which is $0.4\lambda_h$. Note that there is a column of vias for changing the dipole arm layer for tight coupling. Both the dipole and HSB layer are printed on the substrate of Rogers 4003C with the relative permittivity of 3.55 and thickness of 0.305 mm.

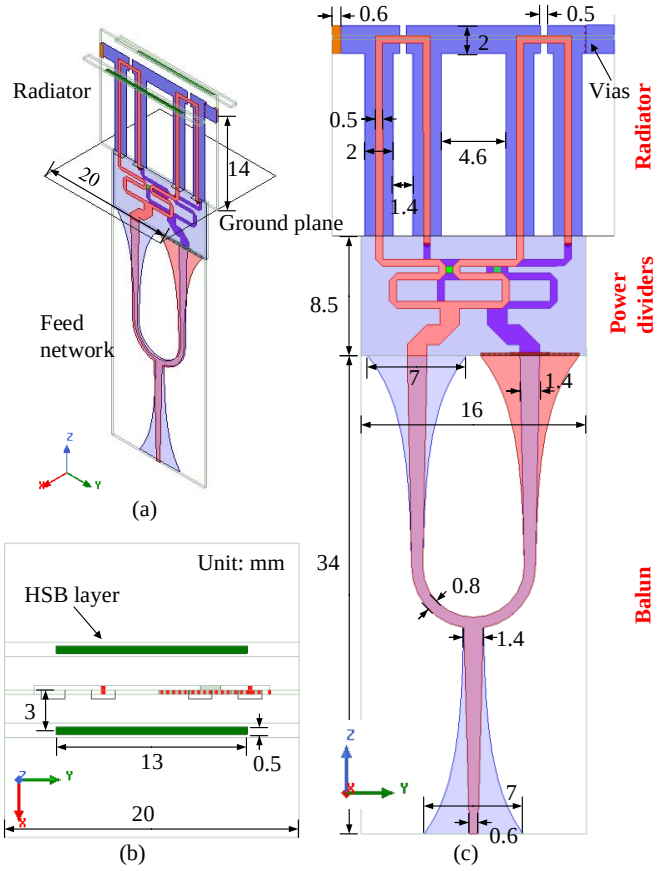

Fig. 1. The proposed differentially fed dual-set TCDA unit cell. (a) 3D view, (b) top view, and (c) Side view.

Fig. 2 shows the detailed configuration of the newly designed feed network below the ground plane. It is composed of the top two back-to-back Wilkinson power dividers and the bottom exponential-tapered baluns. Fig. 2 (a) shows the 3D view of the power dividers. The top four ends are connected to the four ends of the radiator through the ground plane, and the bottom two ends are connected to the tapered baluns for differential feed. Note that two substrates of Roger 4003C with the thickness of 0.305 mm are stacked in the PCB stack, and three copper layers are used in the design of the power dividers. The top layer is shown in pink, and the bottom layer is shown in blue. Two same Wilkinson power dividers are designed on the top and bottom layers, and the center layer is the ground plane. Fig. 2 (b) shows the top view of the power dividers. As can be seen, the power dividers split the input signal into two-way equal magnitude and co-phase signals. The bottom power divider is sheltered by the ground plane, which conducts the signal to the top layer by using two plated through vias.

Fig. 2 (c) shows the top view of the exponentially tapered balun. It splits the input signal into two-way equal-magnitude but out-of-phase signals. The output ports are connected to the top two Wilkinson power dividers, and the input port is connected to an SMA connector for excitation of the unit cell. This balun is composed of two conducting layers, the top layer is shown in pink, and the bottom layer is shown in blue. The substrate of Rogers 4003C with the thickness of 0.305 mm is used in the balun design. The differential output pair is realized by flipping one tapered transmission line upside down. The signal is transmitted to the bottom power divider by a jumper.

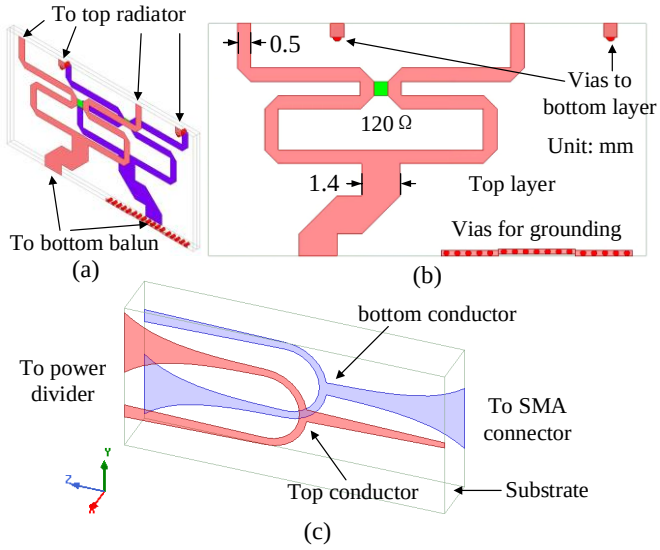

Fig. 2. Configuration of the 1to4 feed network. (a) 3D view. (b) Top view. (c) Exploded view of the tapered differential balun.

B. HSB Layer

In this work, the HSB layer is first proposed to improve the scanning performance in H-plane. TCDA always have an inferior scanning performance in H-plane compared to that in E-plane. Although it is found that the parasitic strips were used in [12], the full potential of working as the HSB layer is firstly investigated and discussed in this work. To show the advantages of using HSB layer, the VSWR of the unit cell when scanning to different angles is shown in Fig. 3 (a), and performance without the HSB layer is added in Fig. 3 (b) for a good comparison. It can be seen that the presented unit cell can have an impedance bandwidth of 1.97-8.05 GHz for VSWR<2 when scanning to the broadside. When scanning to 50° in both E-plane and H-plane, the simulated VSWRs are well below 3 within the bandwidth of 1.89-8.06 GHz. As a good contrast, when the unit cell removes the HSB layer, it has a very similar impedance bandwidth when scanning to the broadside or 50° in E-plane. However, when the unit cell scans to 50° in H-plane, the simulated VSWR is higher than 3, and worst value is around 5.6 at 6.7 GHz. Therefore, the introduction of HSB layer is very efficient to improve the scanning range in H-plane.

The total antenna efficiency of the unit cell with different scanning angles is also investigated and shown in Fig. 4 for a good comparison. As can be seen, the improvement on the total efficiency of the unit cell is also effective and obvious. Without the HSB layer, the total efficiency reduces seriously below 60% when the frequency is higher than 5 GHz. After the introduction of the HSB layer into the unit cell, the total efficiency of the unit cell is improved when the beam scans to the broadside direction, and the majority of values are higher than 80%. Most importantly, the total efficiency for the unit cell scanning to 50°

in H-plane is greatly improved. All the values are higher than 60% within the impedance bandwidth.

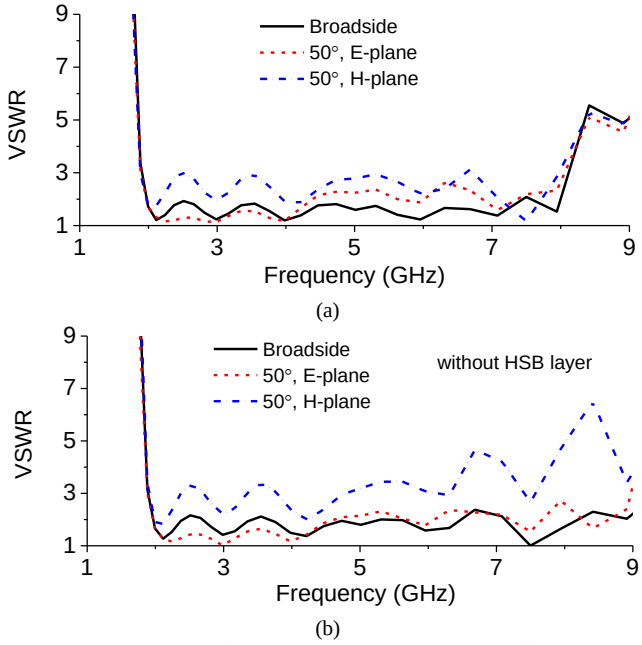

Fig. 3. Simulated VSWR of the unit cell when scanning to different angles (a) with and (b) without HSB layer.

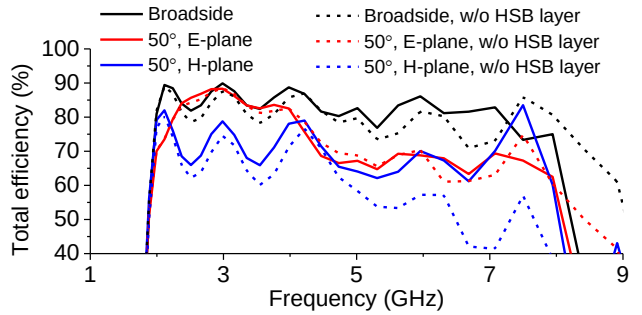

Fig. 4. Simulated total radiation efficiency of the unit cell when scanning to different angles.

C. *Differential Feed*

The proposed unit cell uses the differential feed method to achieve wide impedance bandwidth and low cross-polarization levels. Fig. 5 shows the simulated VSWRs and normalized radiation patterns of the proposed unit cell with the different feed methods. Two different feed methods using four-port differential excitation and Marchand balun are shown on the top of Fig. 5 (a) for structural comparison. For the unit cell excited directly by the differential ports, two pairs of differential port-pair are set at the ends of the microstrip lines to drive the top radiator. For the unit cell fed by the Marchand balun, a classic Marchand balun [9] is designed to excite the top radiator with the same dual-set configuration.

First, as shown in Fig. 5 (a), the VSWR of the unit cell using the proposed feed network shown in Fig. 1 has a very similar impedance bandwidth, as is directly excited by the differential port-pairs. When the practical feed network is introduced, more VSWR ripples are observed within the bandwidth. However, the VSWR<2 bandwidths of two unit cells are almost the same. In contrast, when the Marchand balun is utilized to drive the top radiator, the value of the VSWR is increased and deteriorated. In addition, the lower bandwidth is narrowed as shown in the figure. This shows the limitation of the Marchand balun in impedance transformation for ultra-wide bandwidth.

Fig. 5 (b) shows the difference in the normalized radiation patterns using different feed methods. It can be seen that for the co-polarized radiation patterns in E-plane, they have a good accordance, and are the same as each other. However, for the cross-polarized radiation patterns, the unit cell fed by two direct differential port pairs has the lowest cross-polarization level because of the symmetrical and balanced feed method. The unit cell using Marchand balun has the worst cross-polarization performance due to the slight unbalanced current distributed on the feed lines. The simulated value is higher than -26 dB in the broadside direction. Almost as good as the unit cell fed by ideal differential port-pair, the unit cell fed by the proposed feed network has a very low cross-polarization level. Its value is lower than -42 dB in the broadside direction. Overall, the unit cell using the proposed feed network can have an ultra-wide bandwidth, and keep a low cross-polarization level.

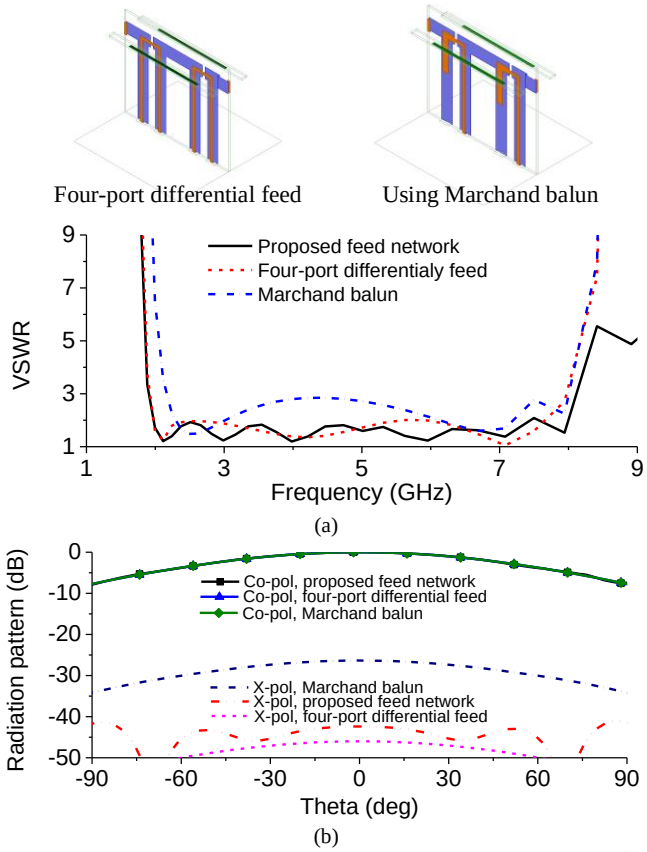

Fig. 5. (a) VSWRs and (b) normalized radiation patterns in E-plane of the proposed unit cell with different feed methods.

III. 5×13 Finite Array

A 5×13 finite array was designed, fabricated, and measured for both impedance and radiation patterns verification based on the designed unit cell. Fig. 6 (a) shows the configuration of the finite array using the proposed unit cell. The total size of the top finite array radiator is 260 mm × 100 mm × 15 mm. Fig. 6 (b) shows a photograph of the fabricated prototype.

A. *Impedance Performance*

The measured active VSWRs of the center element in the fabricated finite array are shown in Fig. 7. The measurement of

the active VSWR follows the general method presented in [7]. As shown in the figure, when the beam is in the broadside direction, the bandwidth is 1.88-8.12 GHz with the active VSWR less than 2.2. As the beam scans to 50° in E-plane, the bandwidth is 1.88-8.36 GHz with the active VSWR less than 3.6. Most importantly, as the beam scans to 50° in H-plane, the bandwidth is 1.84-8.76 GHz with the active VSWR less than 3.6. The simulated active VSWRs are added for comparison, and a good agreement can be seen between the simulated and measured results. The slight tendency difference and multiple ripples are mainly due to the fabrication errors and connected coaxial cables for S-parameters' measurement.

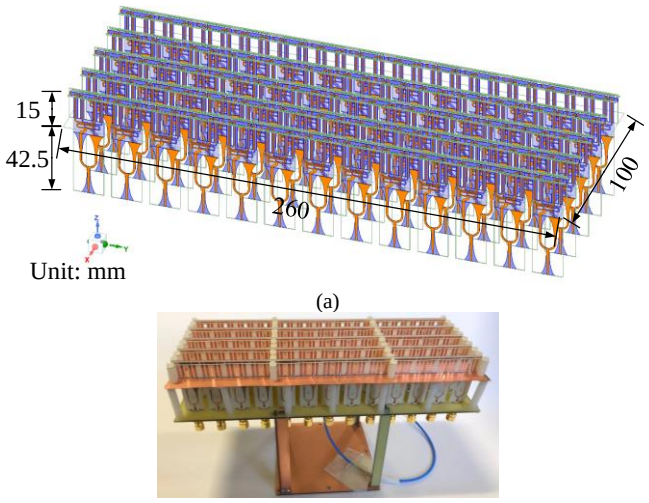

Fig. 6. (a) Configuration and (b) photograph of the fabricated finite array.

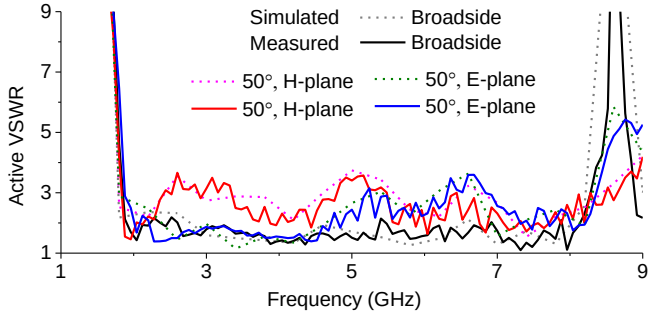

Fig. 7. Measured active VSWRs of the center element in the fabricated finite array under different scan angles.

B. Radiation Performance

The measured broadside peak realized gain and total antenna efficiency of the 5×13 array antenna are shown in Fig. 8. It can be seen that the measured peak realized gain changes nearly linearly from 10 dBi to 21.5 dBi as the increase of frequency. The measured total efficiency varies from 60% to 80%. Overall, the measured peak realized gain and the total efficiency are slightly lower than the simulated results, this minor difference may be due to the introduction of the external feed networks and cables for radiation patterns measurement.

The beam scanning performances of the fabricated 5×13 array antenna are evaluated by the general method based on the unit excitation active element patterns [10]. The measured beam scanning radiation patterns are synthesized through the measured radiation patterns of all the elements. Fig. 9 shows the measured scanning radiation patterns at different frequencies in both E-plane and H-plane. As can be seen, the measured radiation patterns agree well with the simulated radiation patterns at these different frequencies and in different scanning planes. The beam can scan to the desired angles just as the simulated radiation patterns. Owing to the differential feed method, the measured cross-polarization levels keep -30.5 dB lower than the co-polarization levels. The discrepancies between the measured and simulated radiation patterns are mainly due to the fabrication errors, position errors, and the influences of the fixtures and connected cables.

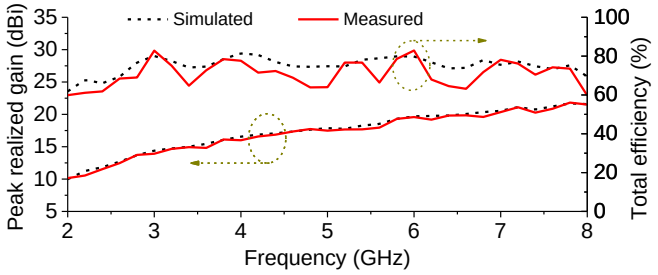

Fig. 8. Measured and simulated peak realized gains and total efficiencies when the beam is in broadside direction.

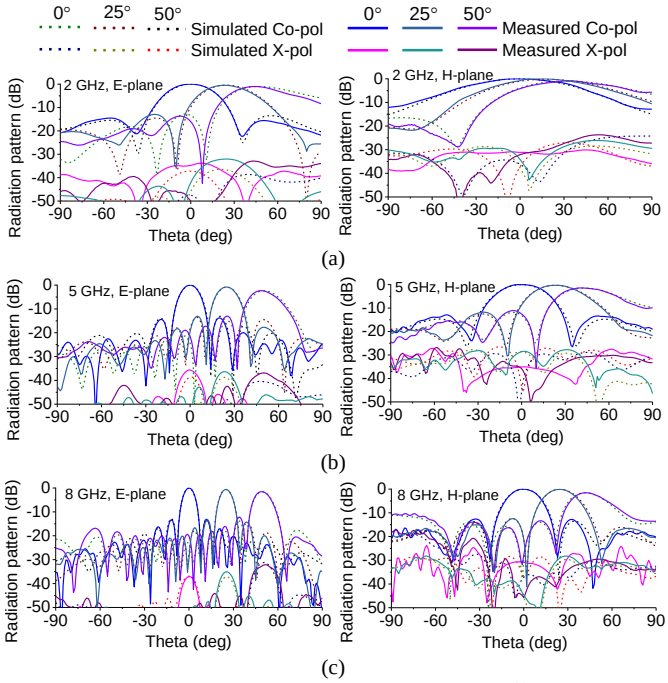

Fig. 9. Measured and simulated radiation patterns with the different scan angles at (a) 2 GHz, (b) 5 GHz, and (c) 8 GHz in E- and H-planes.

IV. Conclusion

This paper proposes a new method to improve the H-plane scanning performance with a newly developed TCDA antenna for WPT applications. The developed TCDA antenna features a consistent and wide scanning performance of ±50° in both E-plane and H-plane with the advantages of low profile, low cost, and light weight. The measured results prove that a wide scanning range of ±50° in both E-plane and H-plane is achieved, which covers the bandwidth of 1.88-8.12 GHz (4.3:1) with a low top-to-ground profile of $0.4\lambda_h$. In addition, owing to the differential feed method, low-cross polarization levels of less than -30.5 dB are achieved. Therefore, the designed TCDA antenna can be a good candidate for WPT applications.

REFERENCES

[1] H. Le-Huu, G. T. Bui, and C. Seo, "Efficient compact radiative near-field wireless power transfer to miniature biomedical implants," *IEEE Antennas Wireless Propag. Lett.*, vol. 22, no. 12, pp. 2803-2807, Dec. 2023.

[2] W. -S. Lee, S. Park, J. -H. Lee and M. M. Tentzeris, "Longitudinally misalignment-insensitive dual-band wireless power and data transfer systems for a position detection of fast-moving vehicles," *IEEE Trans. Antennas Propag.*, vol. 67, no. 8, pp. 5614-5622, Aug. 2019.

[3] P. Lu, C. Song and K. M. Huang, "A two-port multipolarization rectenna with orthogonal hybrid coupler for simultaneous wireless information and power transfer," *IEEE Trans. Antennas Propag.*, vol. 68, no. 10, pp. 6893-6905, Oct. 2020.

[4] C. Song et al., "Highly efficient wideband mmWave rectennas for wireless power transfer system with low-cost multinode tracking capability," *IEEE Trans. Antennas Propag.*, vol. 71, no. 11, pp. 8773-8787, Nov. 2023.

[5] H. Wheeler, "Simple relations derived fom a phased-array antenna made of an infinite current sheet," *IEEE Trans. Antennas Propag.*, vol. AP-13,no. 4, pp. 506–514, Jul. 1965.

[6] B. A. Munk, "Broadband wire arrays," in *Finite Antenna Arrays FSS*, 1st ed. New York, NY, USA: Wiley, 2003, ch. 6, pp. 181–213.

[7] D. K. Papantonis and J. L. Volakis, "Dual-polarized tightly coupled array with substrate loading," *IEEE Antennas Wireless Propag. Lett.*, vol. 15, pp. 325-328, 2016.

[8] Y. Wang, L. Zhu, H. Wang, Y. Luo and G. Yang, "A compact, scanning tightly coupled dipole array with parasitic strips for next-generation wireless applications," *IEEE Antennas Wireless Propag. Lett.,* vol. 17, no. 4, pp. 534-537, April 2018.

[9] S. Zhang, Y. Chen and S. Yang, "An Extremely wideband tightly coupled dipole array with shared-aperture configuration," *IEEE Antennas Wireless Propag. Lett.*, vol. 22, no. 6, pp. 1366-1370, June 2023.

[10] B. Wang, S. Yang, Y. Chen, S. Qu and J. Hu, "Low cross-polarization ultrawideband tightly coupled balanced antipodal dipole array," *IEEE Trans. Antennas Propag.*, vol. 68, no. 6, pp. 4479-4488, June 2020.

[11] C. -H. Hu, B. -Z. Wang, G. -F. Gao, R. Wang, S. -Q. Xiao and X. Ding, "Conjugate impedance matching method for wideband and wide-angle impedance matching layer with 70° scanning in the H-plane," *IEEE Antennas Wireless Propag. Lett.*, vol. 20, no. 1, pp. 63-67, Jan. 2021.

[12] B. Riviere, H. Jeuland and S. Bolioli, "New equivalent circuit model for a broadband optimization of dipole arrays," *IEEE Antennas Wireless Propag. Lett.*, vol. 13, pp. 1300-1304, 2014.

[13] X. Chen and K. Li, "Ultrathin and flexible ultrawideband antenna array based on integrated impedance matching line," *IEEE Antennas Wireless Propag. Lett.*, vol. 22, no. 5, pp. 960-964, May 2023.

[14] J. A. Kasemodel, C. -C. Chen and J. L. Volakis, "Wideband planar array with integrated feed and matching network for wide-angle scanning," *IEEE Trans. Antennas Propag.*, vol. 61, no. 9, pp. 4528-4537, Sept. 2013.

[15] J. P. Doane, K. Sertel and J. L. Volakis, "A wideband, wide scanning tightly coupled dipole array with integrated balun (TCDA-IB)," *IEEE Trans. Antennas Propag.*, vol. 61, no. 9, pp. 4538-4548, Sept. 2013.

[16] S. Xiao, S. Yang, Y. Chen, S. -W. Qu and J. Hu, "An ultra-wideband tightly coupled dipole array co-designed with low scattering characteristics," *IEEE Trans. Antennas Propag.*, vol. 67, no. 1, pp. 676-680, Jan. 2019.

[17] M. H. Novak and J. L. Volakis, "Ultrawideband antennas for multiband satellite communications at UHF–Ku frequencies," *IEEE Trans. Antennas Propag.*, vol. 63, no. 4, pp. 1334-1341, April 2015.

[18] E. Yetisir, N. Ghalichechian and J. L. Volakis, "Ultrawideband array with 70° scanning using FSS superstrate," *IEEE Trans. Antennas Propag.*, vol. 64, no. 10, pp. 4256-4265, Oct. 2016.

[19] H. Zhang, S. Yang, Y. Chen, J. Guo and Z. Nie, "Wideband dual-polarized linear array of tightly coupled elements," *IEEE Trans. Antennas Propag.*, vol. 66, no. 1, pp. 476-480, Jan. 2018.

[20] Z. Jiang, S. Xiao, Z. Yao and B. -Z. Wang, "A planar ultrawideband wide-angle scanning array loaded with polarization-sensitive frequency-selective surface structure," *IEEE Trans. Antennas Propag.*, vol. 68, no. 11, pp. 7348-7357, Nov. 2020.

[21] A. O. Bah, P. -Y. Qin, R. W. Ziolkowski, Y. J. Guo and T. S. Bird, "A wideband low-profile tightly coupled antenna array with a very high figure of merit," *IEEE Trans. Antennas Propag.*, vol. 67, no. 4, pp. 2332-2343, April 2019.

[22] B. Wang, S. Yang, Z. Zhang, Y. Chen, S. Qu and J. Hu, "A ferrite-loaded ultralow profile ultrawideband tightly coupled dipole array," *IEEE Trans. Antennas Propag.*, vol. 70, no. 3, pp. 1965-1975, March 2022.

[23] Z. Zhang, M. Huang, Y. Chen, S. -W. Qu, J. Hu and S. Yang, "In-band scattering control of ultra-wideband tightly coupled dipole arrays based on polarization-selective metamaterial absorber," *IEEE Trans. Antennas Propag.*, vol. 68, no. 12, pp. 7927-7936, Dec. 2020.

[24] L. -H. Wen et al., "Compact dual-polarized shared-dipole antennas for base station applications," *IEEE Trans. Antennas Propag.*, vol. 66, no. 12, pp. 6826-6834, Dec. 2018.